The 2010 IEEE/RSJ International Conference on
Intelligent Robots and Systems
October 18-22, 2010, Taipei, Taiwan

Two-Leveled Obstacle Avoidance Scheme Using a Kinematically Redundant Omni-directional Mobile Robot

Eui-Jung Jung, Sung Mok Kim, Byung-Ju Yi, *Member, IEEE,* and Whee Kuk Kim, *Member, IEEE*

***Abstract*—This work presents the kinematic modeling and motion planning algorithm for an omni-directional mobile robot with kinematic redundancy. This robot consists of three wheel mechanisms each of which has one redundant joint as compared to the operational degrees. Initially, the kinematic modeling of this robot is conducted. Next, using such a kinematic redundancy of each chain, several motion planning algorithms are suggested. A localization algorithm of the mobile robot based on odometry is presented and specifically, two-leveled obstacle avoidance scheme, which simultaneously considers both large and small obstacles, is presented. The usefulness of the proposed algorithms is verified through simulation.**

I. Introduction

FOR a mobile robot to have an omni-directional characteristic on planar space, each wheel mechanism of the robot should generate three degrees of freedom motion. Either the caster wheel or Swedish wheel can be kinematically modeled as three degree of freedom serial chain. Recently, researches on omni-directional mobile robots with active caster wheels have drawn much attention.

Campion, *et al.* [1] proved the omni-directionality of the caster wheel. Wada, *et al.* [2] developed a mobile robot with two caster wheels and one rotational actuator. Yi and Kim [3] initially developed the kinematic model of the omni-directional mobile robot with active caster wheels. Salih, *et al.* [4] developed an omni-directional mobile robot using four custom-made mecanum wheels. Moore and Flann [5] and Berkermeier and Ma [6] implemented a six-wheeled omni-directional mobile robot and ODIS (Omni-Directional Inspection System) with the so-called "smart wheel" active caster wheel module, respectively. Ushimi, *et al.* [7] developed an omni-directional vehicle with two wheels caster. Lee, et al. [8] implemented and proposed a motion generation algorithm for the caster-type omni-directional mobile robot. Park, *et al.* [9] performed the optimal design for the omni-directional mobile robot with caster wheels. Tadakuma, *et al.* [10] proposed a three-wheeled mobile robot that has kinematic redundancy for each chain. However, the mathematical modeling was not provided. Endo and Hirose [11] presented a study on roller-walker in which multi-mode steering control and self-contained locomotion were introduced. This mobile robot also has kinematic redundancy but it is not omni-directional. Davis, *et al.* [12] proposed a mobile robotic system for ground-testing of multi-spacecraft proximity operations. This mobile robot incorporated a 6 DOF parallel robot on the platform to provide kinematic redundancy in the operational space, but not in the wheel chain.

In previous research works related to the omni-directional mobile robot with kinematic redundancy, the kinematic redundancy in the wheel chain is limited or a closed-form kinematic model of such robots has not been provided. Therefore, in this work, the kinematic modeling for an omni-directional mobile robot with multiple kinematic redundancies (see Fig.3) is presented, and various motion planning algorithms that exploit the kinematic redundancy of the wheel chain are suggested.

II. First-order Kinematics

To control the mobile robot as shown in Fig.1, we introduce the first-order kinematics that describes the velocity relation between the center of the platform and all input joints. In Fig.1, XY represent the global reference frame, and xy denote a local coordinate frame attached to the mobile platform; **i**, **j**, and **k** are the unit vectors of the xyz coordinate frame. C denotes the origin of the local coordinate frame.

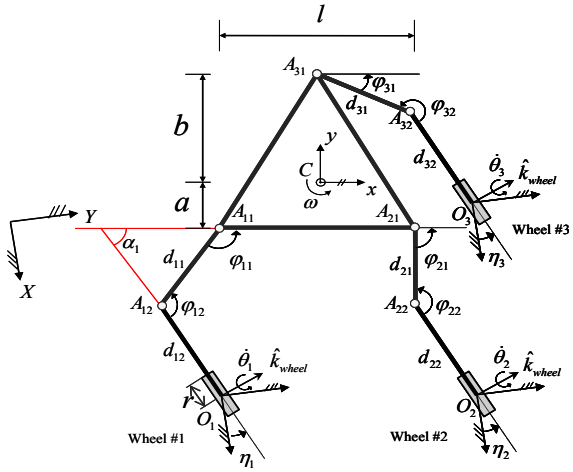

Fig.1. Kinematic description of the omni-directional mobile robot.

E.-J. Jung is with school of Electrical Engineering and Computer Science, Hanyang University, Korea. (e-mail :jeuij79@naver.com)

S.M. Kim is with Department of Control and Instrumentation Engineering, Korea University, Korea. (e-mail :k2potobox@korea.ac.kr)

B.-J. Yi is with school of Electrical Engineering and Computer Science, Hanyang University, Korea. (e-mail:bj@hanyang.ac.kr, corresponding author)

W.K. Kim is with Department of Control and Instrumentation Engineering, Korea University, Korea. (e-mail :wheekuk@korea.ac.kr)

We define θ as the driving angle of the wheel and φ as the revolute joint angle between the neighboring links. η denotes the angular displacement of the wheel relative to the *X*-axis of the global reference frame. *r* and *d* denote the radius of the wheel and the length of the link, respectively. For convenience, α_i, which is the angle of the caster wheel with respect to the *x*-axis of the local coordinate frame, is defined as

$$\alpha_i \triangleq \varphi_{i1} + \varphi_{i2} - \pi \,. \tag{1}$$

Actually, the mobile robot can be visualized as a parallel mechanism, because the instantaneous kinematics of the mobile robot is equivalent to that of a typical parallel robot that is fixed to the ground. Thus, for kinematic analysis of the mobile robot, we employ the intermediate coordinate transfer method [14] that has been used for modeling of parallel mechanisms.

The linear velocity at the center of the *i*-th wheel is given as

$$\mathbf{v}_{oi} = r\dot{\theta}_i\left(\cos\alpha_i\mathbf{i} - \sin\alpha_i\mathbf{j}\right) \quad (i = 1,2,3)\,. \tag{2}$$

The linear velocity at the origin C of the mobile robot can be described as

$$\begin{aligned}\mathbf{v}_c &= \mathbf{v}_{o1} + \dot{\eta}_1\mathbf{k}\times\overrightarrow{O_1A_{12}} + (\dot{\eta}_1+\dot{\varphi}_{12})\mathbf{k}\times\overrightarrow{A_{12}A_{11}} + \omega\mathbf{k}\times\overrightarrow{A_{11}C}\\ &= r\dot{\theta}_1\left(\cos\alpha_1\mathbf{i} - \sin\alpha_1\mathbf{j}\right) + \dot{\eta}_1\mathbf{k}\times d_{12}\left(-\cos\alpha_1\mathbf{i} + \sin\alpha_1\mathbf{j}\right)\\ &\quad + (\dot{\eta}_1+\dot{\varphi}_{12})\mathbf{k}\times d_{11}\left(-\cos\varphi_{11}\mathbf{i} + \sin\varphi_{11}\mathbf{j}\right) + \omega\mathbf{k}\times\left(\frac{l}{2}\mathbf{i} + a\mathbf{j}\right),\end{aligned} \tag{3}$$

$$\begin{aligned}\mathbf{v}_c &= \mathbf{v}_{o2} + \dot{\eta}_2\mathbf{k}\times\overrightarrow{O_2A_{22}} + (\dot{\eta}_2+\dot{\varphi}_{22})\mathbf{k}\times\overrightarrow{A_{22}A_{21}} + \omega\mathbf{k}\times\overrightarrow{A_{21}C}\\ &= r\dot{\theta}_2\left(\cos\alpha_2\mathbf{i} - \sin\alpha_2\mathbf{j}\right) + \dot{\eta}_2\mathbf{k}\times d_{22}\left(-\cos\alpha_2\mathbf{i} + \sin\alpha_2\mathbf{j}\right)\\ &\quad + (\dot{\eta}_2+\dot{\varphi}_{22})\mathbf{k}\times d_{21}\left(-\cos\varphi_{21}\mathbf{i} + \sin\varphi_{21}\mathbf{j}\right) + \omega\mathbf{k}\times\left(-\frac{l}{2}\mathbf{i} + a\mathbf{j}\right),\end{aligned} \tag{4}$$

$$\begin{aligned}\mathbf{v}_c &= \mathbf{v}_{o3} + \dot{\eta}_3\mathbf{k}\times\overrightarrow{O_3A_{32}} + (\dot{\eta}_3+\dot{\varphi}_{32})\mathbf{k}\times\overrightarrow{A_{32}A_{31}} + \omega\mathbf{k}\times\overrightarrow{A_{31}C}\\ &= r\dot{\theta}_3\left(\cos\alpha_3\mathbf{i} - \sin\alpha_3\mathbf{j}\right) + \dot{\eta}_3\mathbf{k}\times d_{32}\left(-\cos\alpha_3\mathbf{i} + \sin\alpha_3\mathbf{j}\right)\\ &\quad + (\dot{\eta}_3+\dot{\varphi}_{32})\mathbf{k}\times d_{31}\left(-\cos\varphi_{31}\mathbf{i} + \sin\varphi_{31}\mathbf{j}\right) + \omega\mathbf{k}\times -b\mathbf{j},\end{aligned} \tag{5}$$

where ω representing the angular velocity of the mobile platform can be described as

$$\omega = \dot{\eta}_i + \dot{\varphi}_{i1} + \dot{\varphi}_{i2}, \quad (i = 1,2,3)\,. \tag{6}$$

Now, $\mathbf{v}_C = \begin{bmatrix} v_{cx} & v_{cy}\end{bmatrix}^T$ and ω can be combined as the operational velocity vector of the omni-directional mobile robot defined by

$$\underline{\dot{u}} = \begin{bmatrix} v_{cx} & v_{cy} & \omega\end{bmatrix}^T. \tag{7}$$

For the first wheel chain, (3) and (6) are expressed as

$$\underline{\dot{u}} = \begin{bmatrix} -d_{12}\sin\alpha_1 - d_{11}\sin\varphi_{11} - a & r\cos\alpha_1 & -a & -d_{11}\sin\varphi_{11} - a\\ -d_{12}\cos\alpha_1 - d_{11}\cos\varphi_{11} + \frac{l}{2} & -r\sin\alpha_1 & \frac{l}{2} & -d_{11}\cos\varphi_{11} + \frac{l}{2}\\ 1 & 0 & 1 & 1\end{bmatrix}\begin{bmatrix}\dot{\eta}_1\\ \dot{\theta}_1\\ \dot{\varphi}_{11}\\ \dot{\varphi}_{12}\end{bmatrix}, \tag{8}$$

for the second wheel chain, (4) and (6) are expressed as

$$\underline{\dot{u}} = \begin{bmatrix} -d_{22}\sin\alpha_2 - d_{21}\sin\varphi_{21} - a & r\cos\alpha_2 & -a & -d_{21}\sin\varphi_{21} - a\\ -d_{22}\cos\alpha_2 - d_{21}\cos\varphi_{21} - \frac{l}{2} & -r\sin\alpha_2 & -\frac{l}{2} & -d_{21}\cos\varphi_{21} - \frac{l}{2}\\ 1 & 0 & 1 & 1\end{bmatrix}\begin{bmatrix}\dot{\eta}_2\\ \dot{\theta}_2\\ \dot{\varphi}_{21}\\ \dot{\varphi}_{22}\end{bmatrix}, \tag{9}$$

and for the third wheel chain, (5) and (6) are expressed as

$$\underline{\dot{u}} = \begin{bmatrix} -d_{32}\sin\alpha_3 - d_{31}\sin\varphi_{31} + b & r\cos\alpha_3 & b & -d_{31}\sin\varphi_{31} + b\\ -d_{32}\cos\alpha_3 - d_{31}\cos\varphi_{31} & -r\sin\alpha_3 & 0 & -d_{31}\cos\varphi_{31}\\ 1 & 0 & 1 & 1\end{bmatrix}\begin{bmatrix}\dot{\eta}_3\\ \dot{\theta}_3\\ \dot{\varphi}_{31}\\ \dot{\varphi}_{32}\end{bmatrix}. \tag{10}$$

(8) - (10) can be expressed as $\underline{\dot{u}} = J_i\underline{\dot{\phi}_i}$, where $\underline{\dot{\phi}_i}$ is a vector of joint parameters. It is noted from (8) through (10) that each wheel has four joint parameters while controlling three outputs, and thus each wheel chain has one kinematic redundancy.

To take the inverse of (8) - (10) that are not square matrices, we take the pseudo inverse as follows

$$\begin{pmatrix}\dot{\eta}_i\\ \dot{\theta}_i\\ \dot{\varphi}_{i1}\\ \dot{\varphi}_{i2}\end{pmatrix} = \underline{\dot{\phi}_i} = J_i^+\underline{\dot{u}}, \quad (i = 1,2,3)\,, \tag{11}$$

where $J^+ = J^T(JJ^T)^{-1}$. For a given operational velocity vector $\underline{\dot{u}}$, we calculate angular velocities of nine input joints through the pseudo inverse of Jacobian in (11). Since η (the angular displacement of the wheel relative to the X-axis of the global reference frame) is a passive parameter, the number of maximum active inputs is 9 out of the total 12 joint parameters. The omni-directional mobile robot has three kinematic redundancies since three output parameters are controlled by using six inputs. Furthermore, if more than six actuators are used in the system, the mobile robot system has force redundancy. Actually, we employ nine actuators (three for each wheel chain) to control this mobile robot developed for experimentation.

III. DYNAMICS

It is known that the particular solution of (11) minimizes the kinetic energy of the *i*-th chain when the inertia matrix is used as a weighting matrix in the pseudo inverse of Jacobian given in (11). A dynamic modeling approach employing Lagrange's form of D'Alembert principle will be employed. To derive the dynamic model of this system, we convert the system into an open-tree structure by cutting joints of close chains. First, by using the Lagrangian dynamic formulation, a dynamic model of each serial chain is evaluated. Next, by using the virtual work, the open chain dynamics can be directly incorporated into a closed chain dynamics.

As shown in Fig.1, one chain of the mobile robot consists of four rigid bodies; one third of the moving platform, two links, and one wheel. Each rigid body has its kinetic energy. The kinetic energy k_i of the *i*-th rigid body can be expressed as

$$k_i = \frac{1}{2}m_i v_{C_i}^T v_{C_i} + \frac{1}{2}{}^i\omega_i^T\,{}^{Ci}I_i\,{}^i\omega_i\,, \tag{12}$$

where the first term is the kinetic energy due to the linear velocity at the center of the mass of the rigid body, and the second term is the kinetic energy due to the angular velocity of the rigid body. Also m_i and ${}^{Ci}I_i$ are mass and inertia matrix

of the *i*-th link, respectively. Therefore, the total kinetic energy of the open chain is the sum of the kinetic energy of all rigid bodies.

$$k = \sum_{i=1}^{n} k_i . \tag{13}$$

The Lagrangian dynamic formulation is described as

$$\frac{d}{dt}\frac{\partial k}{\partial \dot{\theta}} - \frac{\partial k}{\partial \theta} = \underline{\tau}, \tag{14}$$

where $\underline{\tau}$ is the n x 1 joint torque vector, and k is the sum of the whole kinetic energy. Since we assume that the mobile robot moves only in the planar domain, the potential energy is ignored. Now, substituting (13) into (14) yields an open chain dynamics of the *i-th* chain as [13]

$${}_i\mathbf{T}_\phi = \left[{}_i\boldsymbol{I}^*_{\phi\phi} \right] {}_i\underline{\ddot{\phi}} + {}_i\underline{\dot{\phi}}^T \left[{}_i\boldsymbol{P}^*_{\phi\phi\phi} \right] {}_i\underline{\dot{\phi}}, \tag{15}$$

where $\left[{}_i\boldsymbol{I}^*_{\phi\phi} \right]$ and $\left[{}_i\boldsymbol{P}^*_{\phi\phi\phi} \right]$ denote the inertia matrix and the inertia power array referred to the Lagrangian coordinate set, respectively.

The pseudo inverse of Jacobian in (11) can be changed to a weighted pseudo inverse as follows

$$J_i^+ = W^{-1} J_i^T (J_i W^{-1} J_i^T)^{-1}. \tag{16}$$

Specifically, when the inertia matrix $\left[{}_i\boldsymbol{I}^*_{\phi\phi} \right]$ of the *i*-th chain is chosen as the weighting matrix W, it implies that the particular solution minimizes the kinetic energy of the *i*-th chain.

Fig.2 shows the simulation result that describes the comparison of kinetic energy of two weighting matrices when the following trajectory is given as an example.

$$\begin{cases} v_{cx} = 0m/s,\ v_{cy} = 0.3m/s & 0s \le t < 2s \\ v_{cx} = 0.3m/s,\ v_{cy} = 0m/s & 2s \le t < 4s \\ \omega = 0.3rad/s & 0s \le t < 4s \end{cases} \tag{17}$$

The solid line denotes the kinetic energy when the weighting matrix is given as an identity matrix, and the dotted line denotes the kinetic energy when the weighting matrix is given as the inertia matrix. It is noted that less energy is consumed when the inertia matrix is employed. Thus, this inertia weighted pseudo inverse solution is employed in our system.

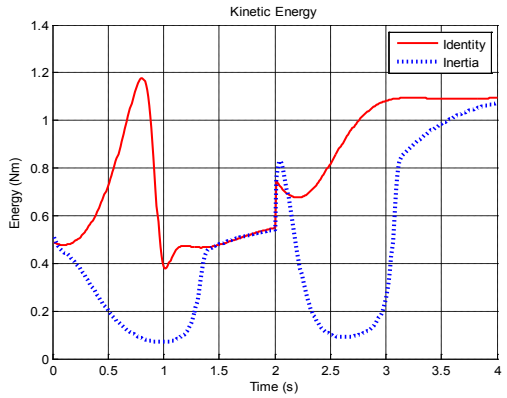

Fig.2. Comparison of kinetic energy of two weighting matrices.

IV. Redundancy Resolution

A. Configuration Changing Algorithm Using Kinematic Redundancy

There are many ways to resolve the motion of each wheel mechanism having one kinematic redundancy. The intermediate coordinate transfer method [14], which has been popularly employed in parallel robot community, cannot be employed to derive the forward kinematic relation because it requires a square Jacobian. Thus, we employ the inertia weighted pseudo inverse solution. Taking the pseudo inverses of (8) - (10), the general solution for each wheel chain is given by

$$\underline{\dot{\phi}_i} = J_i^+ \underline{\dot{u}} + (I - J_i^+ J_i) K \frac{\partial P}{\partial \underline{\phi_i}}, \tag{18}$$

where the scalar function P needs to be optimized. When K is given positive, P is maximized. Otherwise, it is minimized. $\underline{\dot{u}}$ can be any operational velocity vector of the mobile platform.

The merit of this kinematically redundant mobile robot is its versatile motion using the kinematic redundancy of each wheel mechanism. This redundancy in the configuration (or joint) space can be beneficially employed to avoid small obstacles that have low-height in the flat surface. Also the redundancy can be used to obtain the improved dexterity for the given operational pose of the mobile robot.

One such example is the situation that a mobile robot passes through a neck-downed section safely without collision to the obstacle. Here, the desired joint angle φ_{i1d} is decided according to the size of the neck-downed section. Then, the performance index for the *i*-th wheel chain is set as

$$P_A = (\varphi_{i1} - \varphi_{i1d})^2, \tag{19}$$

where we would like to minimize the square of the difference between the current angle φ_{i1} and the desired angle φ_{i1d} of the first joint of the *i*-th wheel chain.

V. Experiment

A. Hardware

Fig.3 shows the proto-type of the kinematically redundant omni-directional mobile robot with three active caster wheels. An embedded robot system should have the ability to compute all the values that the system needs. To implement the embedded mobile robot system, we developed an embedded system that consists of seven DSP controllers, nine motor drivers, a wireless communication module (Bluetooth), and nine actuators with an encoder.

To control all three caster wheels, we embedded the pseudo inverse of Jacobian to two DSP boards for each corresponding chain, and one DSP board is used as the main controller to control the whole system. All DSP boards are connected to each other through CAN. For a given operational velocity vector $\underline{\dot{u}}$, the robot system can be operated in real time.

Fig.3. The omni-directional mobile robot with active caster wheels.

B. Odometry

For navigation, a mobile robot should know its position and orientation with respect to the global reference coordinate. One of fundamental methods for this issue is using its odometer. It can be recognized (see Fig.1) that the components (v_{cx} , v_{cy} , and ω) of the robot operational velocity vector are related to the angular velocity of all the joints by (8) - (10). In our system, we employ nine sensors at nine joints driven by actuator. However, the ground interface variable $\dot{\eta}_i$ in (8) - (10) cannot be measured because they are imaginary joints between wheels and ground. In order to identify such unknown variables, we use the kinematic constraint of the parallel kinematic chains of this mobile robot. If two equations in (8) - (10) are taken, we can calculate the odometry (or pose of the robot). The velocities of the passive joints can be obtained by the following procedure.

For instance, let us consider two wheel chains as shown in Fig.4. Eq. (14) and (15) can be briefly expressed as $\dot{\underline{u}} = J_1\dot{\underline{\phi}}_1$ and $\dot{\underline{u}} = J_2\dot{\underline{\phi}}_2$, respectively. Therefore, the equations are equal as bellows.

$$\dot{\underline{u}} = J_1\dot{\underline{\phi}}_1 = J_2\dot{\underline{\phi}}_2 \tag{20}$$

which can be expressed as

$$\begin{bmatrix} g_{11} & g_{12} & g_{13} & g_{14} \end{bmatrix} \begin{pmatrix} \dot{\eta}_1 \\ \dot{\theta}_1 \\ \dot{\varphi}_{11} \\ \dot{\varphi}_{12} \end{pmatrix} = \begin{bmatrix} g_{21} & g_{22} & g_{23} & g_{24} \end{bmatrix} \begin{pmatrix} \dot{\eta}_2 \\ \dot{\theta}_2 \\ \dot{\varphi}_{21} \\ \dot{\varphi}_{22} \end{pmatrix}, \tag{21}$$

where g_{ij} denotes the *j*-th column of the *i*-th wheel chain's Jacobian. By converting (21), we can obtain the immeasurable variables as follows.

$$\begin{pmatrix} \dot{\eta}_1 \\ \dot{\eta}_2 \end{pmatrix} = \begin{bmatrix} g_{11} & -g_{21} \end{bmatrix}^{+} \begin{bmatrix} -g_{12} & -g_{13} & -g_{14} & g_{22} & g_{23} & g_{24} \end{bmatrix} \begin{pmatrix} \dot{\theta}_1 \\ \dot{\varphi}_{11} \\ \dot{\varphi}_{12} \\ \dot{\theta}_2 \\ \dot{\varphi}_{21} \\ \dot{\varphi}_{22} \end{pmatrix} \tag{22}$$

where + denotes pseudo inverse. Therefore, the operational velocities (v_{cx} , v_{cy} , and ω) are obtained from the (8), (9), and (22). Then, the velocities of the mobile platform can be calculated, with respect to the global reference frame, as bellows.

$$\begin{cases} \dot{x} = v_{cx}\cos(\psi) - v_{cy}\sin(\psi) \\ \dot{y} = v_{cx}\sin(\psi) + v_{cy}\cos(\psi) \\ \dot{\psi} = \omega \end{cases} \tag{23}$$

where x and y are the positions of the mobile platform with respect to the global reference frame, and ψ is the angle between the x axis of the local frame of the mobile robot and the global x-axis.

Finally, the odometry of the mobile robot is implemented by discrete-time integration of (23), such as

$$\begin{cases} x_{k+1} = x_k + Tv_{cxk}\cos(\psi_k + T\omega_k/2) - Tv_{cyk}\sin(\psi_k + T\omega_k/2) \\ y_{k+1} = y_k + Tv_{cxk}\sin(\psi_k + T\omega_k/2) + Tv_{cyk}\cos(\psi_k + T\omega_k/2) \\ \psi_{k+1} = \psi_k + T\omega_k \end{cases} \tag{24}$$

where the subscript *k* denotes the *k-th* time sample and T is the sampling period.

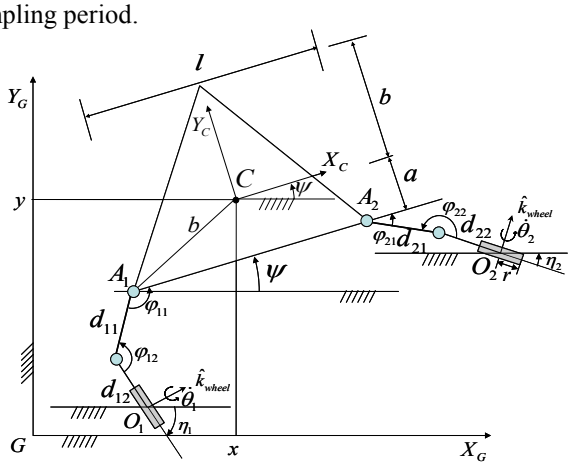

Fig.4. Parameter description for odometry.

C. Experimental results

The attached video clip demonstrates the experimental results for the 3-DOF onmi-directional motion and configuration change while it is moving as shown in Fig.5. The proposed mobile robot is able to create a dexterous omni-directional motion in the planar corridor, and also its redundant joint can be possibly employed to optimize some criterion such as obstacle avoidance. By using (18), (19), and odometry information, the mobile robot can go through a neck-downed section of the corridor successfully.

Fig.5. Configuration change motion at a neck-downed section.

VI. Two-Leveled Obstacle Avoidance Algorithm

A. Navigation Algorithm of the Mobile Platform

The mobile robot that we developed has 3-DOF in the operational space. Thus, more dexterous motion is possible as compared to the 2 DOF differential type mobile robot. The first goal of navigation will be moving the mobile robot to the goal point, and then the second goal will be avoiding obstacles. To satisfy these purposes, positions of the mobile robot, obstacles, and the goal point should be estimated. The navigation algorithm ought to minimize the distance between the current position of the mobile robot and the goal point, and maximize the distances between the current position of the mobile robot and obstacles. The performance indices are then set as follows.

$$\begin{aligned} &\min\{P_G = (x-x_G)^2 + (y-y_G)^2\} \\ &\max\{P_i = (x-x_i)^2 + (y-y_i)^2\}, \end{aligned} \tag{25}$$

where x and y denote the center positions of the mobile robot, x_G and y_G denote the positions of the goal point, and x_i and y_i denote the positions of the i-th obstacle.

Here, we would like to model the omni-directional mobile robot as a kinematically redundant system. Initially, we express the desired angular velocity of the mobile platform in terms of the operational velocity vector $\dot{\underline{u}}$ as follows:

$$\omega_d = J_G \dot{\underline{u}}, \tag{26}$$

where $J_G = \begin{bmatrix} 0 & 0 & 1 \end{bmatrix}$ and $\dot{\underline{u}} = \begin{bmatrix} v_{cx} & v_{cy} & \omega \end{bmatrix}^T$. The general solution for (26) is given by

$$\dot{\underline{u}} = J_G^+ \omega_d + \left(\begin{bmatrix} I \end{bmatrix} - J_G^+ J_G \right) \nabla H, \tag{27}$$

where $J_G^+ = J_G^T (J_G J_G^T)^{-1}$, and H used in the homogeneous solution is the potential function that needs to be optimized. When the gradient of H is given as follows

$$\nabla H = \left(K_G \frac{\partial P_G}{\partial \lambda}^T + \sum K_i \frac{\partial P_i}{\partial \lambda}^T \right), \tag{28}$$

it implies that P_G and P_i are to be optimized. Depending upon the sign of the coefficients K_G and K_i, the mobile robot is controlled in such a way to minimize or maximize the given performance index. In this example, K_G should be negative to minimize the distance between the robot and the goal, and K_i should be positive to maximize the distance between the robot and the obstacles. In (27), if the angular velocity ($\omega_d = 0$) of the mobile robot is given as zero, the mobile robot maintains its initial posture during navigation. Only the homogeneous solution exists in (27), which makes the mobile robot navigate toward the goal while avoiding obstacles.

Decision of K_G and K_i is made as follows. The coefficient K_G related to moving to the goal is determined by experiment like the p-gain of proportional control. The coefficient K_i related to the obstacle avoidance is determined by the following equation.

$$K_i = k e^{\frac{\ln(0.01)}{h} S_i}, \tag{29}$$

where k denotes a weighting factor, h denotes a permissible approach range, and S_i denotes the distance between the mobile robot and the i-th obstacle. K_i is equal to $0.01k$ at $S_i = h$ according to (29). K_i should vary with respect to the distance from an obstacle to the robot, because obstacles outside of the permissible range are not needed to be cared. On the contrary, the obstacle avoidance algorithm is effective for the nearer obstacles. Therefore, the omni-directional mobile robot can avoid obstacles and move to the goal point by applying the operational velocity vector $\dot{\underline{u}}$ generated by (27) to (18).

B. Low-height Obstacle Avoidance Algorithm

When the heights of obstacles strewn on the floor are sufficiently low, the mobile robot could use the self motion of the kinematically redundant caster wheel to avoid those obstacles without affecting the platform motion of the mobile robot. To change the position of the caster wheel, the passive steering angle as well as its wheel rotational angle needs to be controlled like steering a bicycle. Fig.6 illustrates a collision avoidance scheme of the caster wheel with kinematic redundancy, where every obstacle shown in the figure is assumed to be located at low-height. The following describes the summary of the algorithm.

First, in Fig.6, we define a searching range of the caster wheel. The magnitude of this searching range (i.e., angles η_{min} and η_{max}, and the distance R from the wheel shown in the figure) could be selected by considering the normal rotational speed of the wheel and the maximum steering speed. Then, we find the largest angles between obstacles (including maximum and minimum angle ranges), and steer the wheel toward the center, η_d, of the largest obstacle-free sector in the searching range. We note that depending on the rotational direction of the wheel, either the front side or the rear side is searched.

To perform this algorithm, we set the performance index as follows

$$P_B = (\eta_i - \eta_{id})^2. \tag{30}$$

Since η_i is a passive joint angle in Fig.4, we should express it as the function of active joint parameters given by

$$\eta_i = \psi - \varphi_{i1} - \varphi_{i2} + \pi. \tag{31}$$

Then, the performance index is expressed as

$$P_B = (\psi - \varphi_{i1} - \varphi_{i2} + \pi - \eta_{id})^2. \tag{32}$$

Finally, the general solution of this algorithm is given as follows

$$\dot{\underline{\phi_i}} = J_i^+ \dot{\underline{u}} + (I - J_i^+ J_i) \left(-K_B \frac{\partial P_B}{\partial \underline{\phi_i}} \right). \tag{33}$$

Particularly, in the situation such as either obstacles completely block the motion passage of the wheel or the

mobile robot is at internal kinematic singularities, the wheel rotation needs to be drastically reduced (If necessary, it should be stopped) while the steering angle of the wheel is continuously changed to secure a free passage of the wheel around.

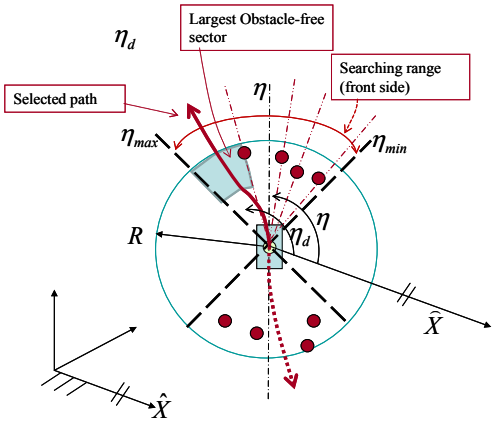

Fig.6. Wheel steering action.

C. Simulation

In this section, we simulate the proposed motion planning algorithms for the kinematically redundant omni-directional mobile robot. Fig.7 shows the simulation result of the motion planning algorithm presented in this section. In the simulation shown in Fig.7, two-leveled obstacle avoidance scheme is employed by applying (25) and (32) as performance indices. The mobile robot moves to the goal point that is located at 10m distance from the staring position, while avoiding large- and small-sized obstacles. One hundred small obstacles are randomly scattered in $100m^2$.

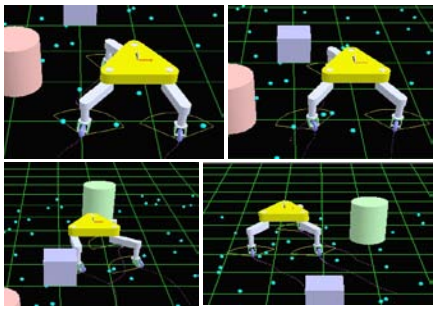
Fig.7. Two-leveled obstacle avoidance scheme.

The attached video clip clearly demonstrates the usefulness of the proposed redundant mobile robot exploiting the kinematic redundancy of each wheel mechanism.

VII. Conclusions

This work proposes the closed-form kinematic model and redundancy resolution algorithms for an omni-directional mobile robot having multiple kinematic redundancies. A localization algorithm of the mobile robot based on odometry is also presented.

We demonstrated through experiment and simulation that such kinematic redundancy could be applied to optimize several performance indices. Specifically, two-leveled obstacle avoidance algorithm was successfully tested. Several subtasks exploiting the kinematic redundancy of this mobile robot will be implemented to the real hardware in the near future.

Acknowledgment

This work was partially supported by Mid-career Researcher Program through NRF grant funded by the MEST (No. 2010-0000247), partially supported by GRRC program of Gyeonggi Province (GRRC HANYANG 2010-A02), partially supported by the Ministry of Knowledge Economy (MKE) and Korea Industrial Technology Foundation (KOTEF) through the Human Resource Training Project for Strategic Technology, and the outcome of a Manpower Development Program for Energy & Resources supported by the Ministry of Knowledge and Economy (MKE).

References

[1] C. Campion, G. Batin, and B.D'Andrea-Novel, "Structural properties and classification of kinematics and dynamics models of wheeled Mobile Robot," *IEEE Trans. on Robotics and Automation*, vol. 4, no. 2, pp. 281–340, 1987.

[2] M. Wada, A. Takagi, and S. Mori, "Caster drive mechanism for holonomic and omnidirectional mobile platforms with no over constraint," in *Proc. IEEE Int. Conf. on Robotics and Automation*, pp. 1531-1538, 2000.

[3] B.-J. Yi and W.K. Kim, "The kinematics for redundantly actuated omni-directional mobile robots," *Journal of Robotic Systems*, vol. 19, no. 6, pp. 255-267, 2002.

[4] J.E.M. Salih, et al., "Designing omni-directional mobile robot with mecanum wheel," *American Journal of Applied Sciences*, vol. 3, no.5, pp. 1831-1835, 2006.

[5] K.L. Moore and N.S. Flann, "A six-wheeled omnidiretional autonomous mobile robot," *IEEE Control System Magazine*, vol. 20, no. 6, pp. 53-66, 2000.

[6] M.D. Berkemeier and L. Ma, "Discrete control for visual servoing the ODIS robot to parking lot lines," in *Proc. IEEE Int. Conf. on Robotics and Automation*, pp. 3149-3154, 2005.

[7] N. Ushimi, M. Yamamoto, and A. Mohri, "Two wheels caster type odometer for omni-directional vehicles," in *Proc. IEEE Int. Conf. on Robotics and Automation*, pp. 497-502, 2003.

[8] J.H. Lee, S. Yuta, E. Koyanagi, and B.-J. Yi, "Command system and motion control for caster-type omni-directional mobile robot," in *Proc. IEEE/RSJ Int. Conf. on Intelligent Robots and Systems*, pp. 2714-2720, 2005.

[9] T.B. Park, J.H. Lee, B.-J. Yi, W.K. Kim, B.J. You, and S.R. Oh, "Optimal design and actuator sizing of redundantly actuated omni-directional mobile robots," in *Proc. IEEE Int. Conf. on Robotics and Automation*, pp. 732-737, 2002.

[10] K. Tadakuma, M. Masatsugu, and S. Hirose, "Mechanical design of joint braking and underactuated mechanism of "Tri-Star3"; horizontal polyarticular arm equipped 3-wheeled expandable mobile robot," in *Proc. IEEE/RSJ Int. Conf. on Intelligent Robots and Systems,* pp. 4252-4259, 2006.

[11] G. Endo and S. Hirose, "Study on roller-walker (multi-mode steering control and self-contained locomotion)," in *Proc. IEEE Int. Conf. on Robotics and Automation*, pp. 2808-2814, 2000.

[12] J. Davis, J. Doebbler, J.L. Junkins, and J. Valasek, "Mobile robotic system for ground-testing of multi-spacecraft proximity operations," AIAA-2008-6548, *Proc. AIAA Int. Conf. on Modeling and Simulation Technologies*, August 2008.

[13] K.H. Hunt, *Kinematic Geometry of Mechanisms*, Clarendon Press, Oxford, 1990.

[14] R.A. Freeman and D. Tesar, "Dynamic modeling of serial and parallel mechanisms/robotic systems," Part I-Methodology, Part II-Applications, *20th ASME Biennial Mechanism Conf.*, Orlando, FL, pp. 7-27, 1988.